Available online at www.sciencedirect.com
ScienceDirect
Landscape and Urban Planning 85 (2008) 85–96
LANDSCAPE AND URBAN PLANNING
www.elsevier.com/locate/landurbplan

Assessing the effect of landcover changes on air temperatu×re using remote sensing images—A pilot study in northern Taiwan

Ke-Sheng Cheng [a,*], Yuan-Fong Su [a], Fang-Tzu Kuo [a], Wei-Chun Hung [a], Jie-Lung Chiang [b]

[a] *Department of Bioenvironmental Systems Engineering, National Taiwan University, Taipei, Taiwan, ROC*
[b] *Department of Soil and Water Conservation, Ping-Tung University of Science and Technology, Ping-Tung, Taiwan, ROC*

Received 17 February 2007; received in revised form 15 July 2007; accepted 28 September 2007
Available online 26 November 2007

Abstract

Extensive conversion of paddy fields to other landuse/landcover types may have adverse consequences including microclimate change. In this study we assess the effect of landcover changes on ambient air temperature using remote sensing images. NOAA AVHRR thermal images were used for surface temperature retrieval using the split window technique. SPOT multispectral images were used for landcover classification using the supervised maximum likelihood classification method. Through an inversion algorithm, landcover-specific surface temperatures were estimated. Locally calibrated relationships between surface and air temperatures with respect to different landcover types were developed using field data and used to yield average air temperatures over individual NOAA pixels. Significant linear relationships were found between average air temperatures and within-pixel coverage ratios of individual landcover types. Such relationships are inter-related and they collectively characterize the prevalent landcover conversion pattern in the region. Quantitative assessment of the effect of landcover changes on ambient air temperature was conducted by considering conditions under the prevalent landcover conversion and forced landcover conversion. Under the prevalent landcover conversion, reducing the within-pixel coverage ratio of paddy fields from the maximum of 26% to none will result in an ambient air temperature rise of 1.7–3.1 °C. Forced landcover conversion contradict the existing landcover pattern and may cause complicated consequences. Additional resources allocation and incentives may need to be introduced in order to ensure a successful forced conversion.

Keywords: Landcover conversion; Remote sensing; Air temperature; Northern Taiwan

1. Introduction

Rice cultivation through paddy irrigation has had a long history in eastern and southeastern Asia. The vast extent of paddy fields necessitates a well-organized and sophisticated irrigation network including reservoirs, ponds, intake/outlet structures, pumps, channels, and flumes to convey enough water to all points in an irrigation district. Despite of its long history and relevant cultural aspect, such practices have been criticized for inefficiency of water utilization. In addition, demand and request for larger share of water utilization from industrial sectors are ever increasing due to low market prices of agricultural produce as compared to industrial products. After entering WTO, agricultural sectors in Taiwan also face harsh competition of imported produce from labor-cheap countries. As a result, paddy fields in some regions are left fallow and converting paddy fields to other landuse types have been discussed. However, in addition to rice production, there are also concerns about multifunctionality of paddy cultivation. Such concerns have been the focus of countries and professional societies in eastern and southeastern Asia over the last several years. An important and apparent function of paddy field is its capability of flood retention during the typhoon and monsoon seasons (Nakanishi, 2004; Unami and Kawachi, 2005). Other functions of paddy culture include recharge of groundwater (Greppi, 2004), air temperature cooling (Saptomo et al., 2004; Yokohari et al., 1997, 2001), removal of pollutants in irrigation water (Ishikawa et al., 2003; Nakasone, 2003), providing habitat for inhabitants (Fukuda et al., 2006), aesthetic landscape, and facilitating religious/cultural activities. Many of these functions have been experienced or practiced for many generations. However, quantitative evaluations of individual functions are difficult and rare due to lack

* Corresponding author. Tel.: +886 2 2366 1568; fax: +886 2 2363 5854.
E-mail addresses: rslab@ntu.edu.tw (K.-S. Cheng), williams14.tw@yahoo.com.tw (Y.-F. Su), r92622025@ntu.edu.tw (F.-T. Kuo), r92622038@ntu.edu.tw (W.-C. Hung), jlchiang@mail.npust.edu.tw (J.-L. Chiang).

0169-2046/$ – see front matter © 2007 Elsevier B.V. All rights reserved.
doi:10.1016/j.landurbplan.2007.09.014

of data and, in some cases, difficulty in determining what to measure.

Many major cities in eastern Asia still have paddy fields within their close vicinities. Existence of such paddy fields provides many functions in urban areas (Yokohari et al., 1994). Extensive landuse changes of paddy fields may have significant environmental, ecological, cultural, and social impacts and yield potentially severe and adverse consequences. Therefore, the positive and adverse effects of paddy culture should be thoroughly investigated and considered in the landuse planning and decision-making process.

Yokohari et al. (1994, 1997, 2001) conducted a series of studies on the temperature cooling effect of paddy fields in urban fringe areas of Tokyo using field measured land surface and air temperatures. They found that measured surface temperatures varied by approximately 20 °C, while measured air temperatures differed by more than 2 °C. For large study areas, it would be labor and time consuming to conduct field measurements. With the availability of many images from weather and land observation satellites, it seems beneficial and feasible to use remote sensing images to aid in similar studies. In addition, what kinds of landuse conversions should be pursued in order to avoid adverse effect and to sustain the environmental quality in the region must also be investigated for a sound decision making. Therefore, the objectives of this study are to quantitatively evaluate the effect of landcover types on ambient air temperature using remote sensing images and to understand the inter-relationships of different landcover types in a region through a pilot study conducted in northern Taiwan.

2. Energy exchange between the land surface and the atmosphere

Surface of paddy fields (partly to fully covered by crop canopy, depending on the growth condition) generally has a lower temperature than landcover types like bare soil and paved surfaces due to its higher moisture content in soils. However, instead of the land surface temperature, the ambient air temperature is of interest in assessment of the cooling effect of paddy field. The relationship of land surface temperature and ambient air temperature depends on landcover types and can be derived by considering energy exchange between the atmosphere and the land surface.

Energy exchange between the atmosphere and the land surface (or the crop canopy) can be expressed by the following energy balance equation:

$$R_n - \mathrm{LE} - H - G = 0 \tag{1}$$

where R_n, LE, H and G respectively, represent the net radiation at the land surface, the latent heat flux, the sensible heat flux, and the soil heat flux.

The net radiation is the sum of incoming and outgoing short and longwave radiations on the land surface, and is expressed by

$$R_n = (1 - r_{ss})S_0 - \varepsilon_s \sigma T_s^4 + (1 - r_{sl})\varepsilon_a \sigma T_{sky}^4 \tau \tag{2}$$

In the above equation S_0 is the incident solar radiation, r_{ss} and r_{sl} are respectively the shortwave and thermal (longwave) reflectance of the land surface, ε_s and ε_a are respectively thermal emissivities of the land surface and the atmosphere, and T_s and T_{sky} are respectively the absolute temperature of the canopy or land surface and the atmosphere. τ represents the average transmittance of the atmosphere and σ is the Stefan–Boltzmann constant. The first term in the right-hand-side of the above equation is the net incoming shortwave radiation. The second term is the thermal radiation emitted from the land surface. The last term is the thermal radiation emitted by the atmosphere and absorbed by the land surface. For thermal radiation, transmittance through the land surface can be assumed to be zero and, under the thermal equilibrium, the emissivity equals the absorptance (α_s). Therefore,

$$\alpha_s + r_{sl} = \varepsilon_s + r_{sl} = 1 \tag{3}$$

The net radiation of the land surface R_n can thus be expressed as

$$R_n = (1 - r_{ss})S_o - \varepsilon_s \sigma T_s^4 + \varepsilon_s \varepsilon_a \sigma T_{sky}^4 \tau \tag{4}$$

The sensible heat flux can be expressed in terms of temperature difference as (Monteith and Unsworth, 1990):

$$H = \rho C_p \frac{T_s - T_a}{r_a} \tag{5}$$

where ρ is the air density, C_p the specific heat of air at constant pressure, r_a the aerodynamic resistance, and T_a is the air temperature at a reference height above the land surface.

The latent heat is the energy used for transport of water vapor from the land surface, through crop evapotranspiration or evaporation from the soil, to the atmosphere and may be expressed as (Monteith and Unsworth, 1990):

$$\mathrm{LE} = \frac{\rho C_p [e_0(T_s) - e_a]}{r_a \gamma} \tag{6}$$

where $e_0(T_s)$ is the saturation vapor pressure at temperature T_s, e_a is the actual vapor pressure, and γ is the psychrometric constant. The vapor pressure deficit (VPD) of the atmosphere is defined as

$$\mathrm{VPD} = e_0(T_a) - e_a \tag{7}$$

The $e_0(T_s) - e_a$ term in Eq. (6) can be expressed by

$$e_o(T_s) - e_a = [e_o(T_a) - e_a] + \Delta(T_s - T_a) \tag{8}$$

where Δ is the slope of the saturation vapor pressure as a function of temperature. Substituting Eq. (8) into Eq. (6), it yields:

$$\mathrm{LE} = \frac{\rho C_p [\mathrm{VPD} + \Delta(T_s - T_a)]}{r_a \gamma} \tag{9}$$

Idso et al. (1997) suggested that the soil heat flux (G) can be considered as a fraction (ξ) of R_n, i.e.,

$$G = \xi R_n \tag{10}$$

Rearrangement of the energy balance equation, i.e. Eq. (1), yields:

$$(1-\xi)R_n = H + LE \tag{11}$$

Substituting Eqs. (5) and (9) into Eq. (11), we have

$$(1-\xi)R_n = \rho C_p \frac{T_s - T_a}{r_a} + \frac{\rho C_p[VPD + \Delta(T_s - T_a)]}{r_a \gamma} \tag{12}$$

Rearranging the above equation yields:

$$\left[1 + \frac{\Delta}{\gamma}\right](T_s - T_a) = \frac{r_a(1-\xi)R_n}{\rho C_p} - \frac{VPD}{\gamma} \tag{13}$$

$$T_a = T_s - \left[\frac{r_a \gamma (1-\xi)R_n}{(\Delta+\gamma)\rho C_p} - \frac{VPD}{\Delta+\gamma}\right] \tag{14}$$

The above equation expresses the relation of the air and surface temperatures. Both the land surface temperature T_s and the net radiation R_n vary with landcover types, and therefore, the $T_s \sim T_a$ relationships are landcover-dependent. The best way of collecting the landcover information in a large study area is by using remote sensing images, and thus Eq. (14) provides the rationale of combining remotely sensed land surface temperature T_s and locally calibrated $T_s \sim T_a$ relationship for estimation of the air temperature with respect to different landcover types.

3. Study area and remote sensing data set

An area of approximately 275 km^2 in Tao-Yuan County of northern Taiwan was chosen for this study (Fig. 1). It encompasses different landcover types including paddy field, water ponds, residential and factory buildings, and other vegetations. The western half is mostly agricultural area while the eastern half has mixed land uses including manufactural and industrial parks, densely populated residential blocks, and agricultural areas. Multispectral remote sensing images of the study area from NOAA-16 AVHRR sensors and SPOT-4 HRVIR sensors were collected. Overpasses of the NOAA satellites were almost concurrent with the time of field data collection on 16 March and 4 April 2005. NOAA thermal images (channels 4 and 5, with a spatial resolution of 1.1 km × 1.1 km) were used for retrieval of land surface temperature. High-resolution multispectral SPOT images (green, red, and near infrared channels, with a spatial resolution of 20 m × 20 m) were used for landcover classification. A set of 45 orthorectified aerial photos (Fig. 2) at 1:5000 scale were also collected to assist in landcover classification.

4. Land surface temperature estimation using NOAA images

The first step of our approach for assessing the effect of landcover types on ambient air temperature is to estimate the land surface temperatures using NOAA thermal images. The AVHRR sensors aboard NOAA satellites receive and record thermal emissions from objects on the land surface. These sensors receive radiances within specific spectral windows and techniques have been developed for retrieval of land surface temperatures from remote sensing thermal images (Prabhakara et al., 1974; McMillan, 1975; Chedin et al., 1982; Price, 1984; Kerr et al., 1992; Li and Becker, 1993; Vasquez et al., 1997). Among these methods, the split window technique (SWT) briefly described below is most widely applied and is adopted in this study. Readers are referred to Schott (1997) for theoretical details of the following derivations.

Let the radiance received by a sensor with spectral window centered at wavelength λ and the radiance emitted by a tar-

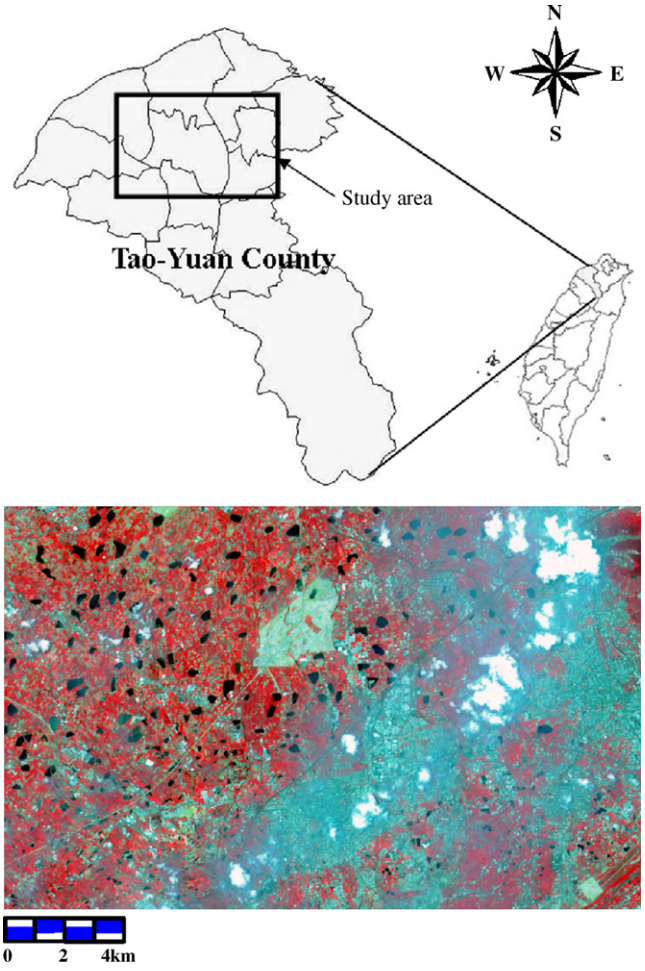

Fig. 1. Location map and pseudo-color SPOT image of the study area.

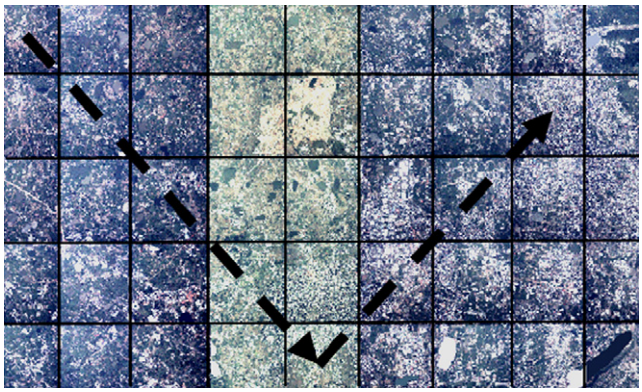

Fig. 2. Orthorefectified aerial photos of the study area and the field sampling route.

get object on the earth surface be respectively represented by $L_\lambda(h)$ and $L(0)$. The radiance from the air column between the target and the sensor due to its mean effective temperature is represented by L_{TA}. We then have

$$L_\lambda(h) = L(0)\tau_\lambda(h) + L_{TA}[1 - \tau_\lambda(h)] \tag{15}$$

where h is the height of the satellite orbit and $\tau_\lambda(h)$ is the effective transmittance of the air column with respect to the sensor's spectral window.

For atmospheres dominated by absorption effects, the transmittance can be expressed as

$$\tau_\lambda(h) = e^{-\beta_\alpha(\lambda)h} \tag{16}$$

where $\beta_\alpha(\lambda)$ is the absorption coefficient with respect to the spectral window centered at λ and $\beta_\alpha(\lambda)h$ is the optical depth. For clear atmospheres, $\tau_\lambda(h)$ can be expanded using a Taylor series and truncated to yield as a good approximation:

$$\tau_\lambda(h) \approx 1 - \beta_\alpha(\lambda)h \tag{17}$$

Therefore,

$$L_\lambda(h) = L(0) - [L(0) - L_{TA}]\beta_\alpha(\lambda)h \tag{18}$$

Assuming linear relationship between the radiance and the apparent temperature, it yields:

$$T_\lambda(h) \approx T(0) - [T(0) - T_A]\beta_\alpha(\lambda)h \tag{19}$$

where $T_\lambda(h)$ is the apparent temperature at the sensor, $T(0)$ the apparent temperature at the surface, and T_A is the apparent temperature corresponding to L_{TA}. The apparent temperature (also known as the brightness temperature) of an object is the kinetic temperature which a perfect radiator would be required to maintain in order to generate the radiance measured from the object.

Suppose that images of two spectral channels (each of nominal wavelength λ_1 and λ_2) within an atmospheric window are available. Then,

$$T_{\lambda_1}(h) = T(0) - [T(0) - T_A]\beta_\alpha(\lambda_1)h \tag{20}$$

$$T_{\lambda_2}(h) = T(0) - [T(0) - T_A]\beta_\alpha(\lambda_2)h \tag{21}$$

where $T_{\lambda_1}(h)$ and $T_{\lambda_2}(h)$ are the apparent temperatures at the sensor with respect to channels 1 and 2, respectively. Rearranging Eqs. (20) and (21), we have

$$T(0) = T_{\lambda_1}(h) + [T(0) - T_A]\beta_\alpha(\lambda_1)h \tag{22}$$

$$T(0) - T_A = \frac{T(0) - T_{\lambda_2}(h)}{\beta_\alpha(\lambda_2)h}, \tag{23}$$

$$T(0) = T_{\lambda_1}(h) + \frac{T(0) - T_{\lambda_2}(h)}{\beta_\alpha(\lambda_2)h}\beta_\alpha(\lambda_1)h \tag{24}$$

$$= T_{\lambda_1}(h) + (T(0) - T_{\lambda_2}(h))\frac{\beta_\alpha(\lambda_1)}{\beta_\alpha(\lambda_2)} \tag{25}$$

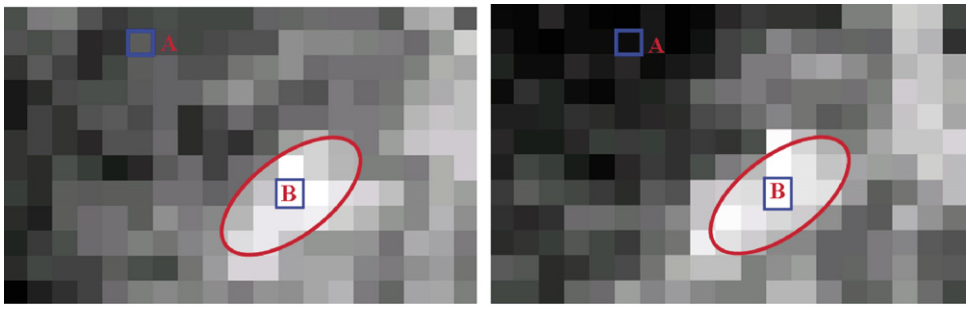

(a) March 16, 2005 (b) April 4, 2005

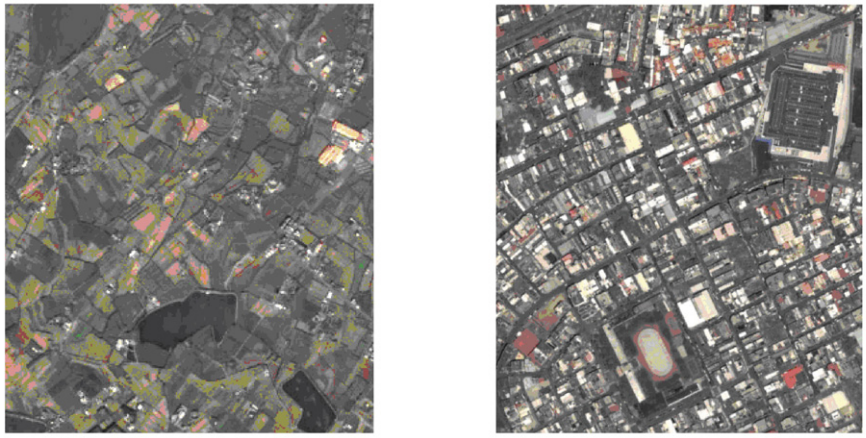

(c) Detailed landcover in area A. (d) Detailed landcover in area B.

Fig. 3. (a) and (b): spatial variation of apparent surface temperatures derived from NOAA AVHRR images. Brighter pixels have higher apparent temperatures. (c) Area A with paddy and other vegetations. (d) Area B with residential and factory buildings.

Let

$$R = \frac{\beta_\alpha(\lambda_1)}{\beta_\alpha(\lambda_2)}, \tag{26}$$

it yields:

$$(1 - R)T(0) = T_{\lambda_1}(h) - T_{\lambda_2}(h)R \tag{27}$$

$$T(0) = \frac{T_{\lambda_1}(h) - RT_{\lambda_2}(h)}{1 - R} \tag{28}$$

$$\begin{aligned} T(0) &= c_1 T_{\lambda_1}(h) + (1 - c_1)T_{\lambda_2}(h) \\ &= c_1 T_{\lambda_1}(h) + c_2 T_{\lambda_2}(h), \quad [c_1 + c_2 = 1] \end{aligned} \tag{29}$$

Or,

$$T(0) = T_{\lambda_1}(h) + \frac{R}{1 - R}[T_{\lambda_1}(h) - T_{\lambda_2}(h)] \tag{30}$$

Eq. (30) shows that the land surface temperature can be calculated using the at-sensor apparent temperatures (which can be calculated using the measured radiances and the Planck's equation) of two spectral channels.

Gallo et al. (1993) and Florio et al. (2004) proposed the following equation for estimation of the land surface temperature using NOAA images of channels 4 and 5.

$$T(0) = T_4 + 3.3(T_4 - T_5) \tag{31}$$

where T_4 and T_5 are respectively the apparent temperatures of the target object derived from NOAA images of channels 4 and 5. Hereafter, apparent surface temperatures estimated using Eq. (31) will be referred to as the SWT surface temperatures.

Fig. 3 shows the spatial variation of SWT surface temperatures over the study area during 2 days of field data collection (described later). It can be seen clearly that apparent surface temperatures are higher in areas with residential and factory buildings (the circled area) and lower in the northwestern region where paddy fields and other vegetations are the dominant landcover types. However, NOAA AVHRR images have a spatial resolution of 1.1 km and each pixel corresponds to an area of 1.21 km^2 on the earth surface. There may be different landcover types within the spatial coverage of a NOAA pixel, and the SWT surface temperatures are average temperatures of all landcover types within the pixel coverage.

5. Estimating the landcover-specific surface temperatures

SWT surface temperatures derived from NOAA images represent average temperatures within a pixel which may be composed of several landcover types. Four major landcover types are present in the study area: (1) paddy fields, (2) water ponds, (3) built-up areas (including paved roads, residential area, and factory buildings) and bare soils, and (4) other vegetations. In order to assess the effect of landcover types on ambient air temperatures, it is necessary to further estimate the apparent temperatures of individual landcover types from the SWT surface temperatures. This can be done by determining the coverage ratios of different landcover types within individual NOAA pixels using the multispectral SPOT images. Detailed procedures are described below.

Assume that k different landcover types are present in the study area. Within the spatial coverage of a pixel, each landcover type accounts for $w_i (i = 1, 2, \ldots, k)$ coverage ratio of the total pixel coverage and the apparent temperatures of different landcover types are represented by $T_i (i = 1,2,\ldots,k)$. The pixel-average land surface temperatures can thus be calculated as

$$\bar{T}(j) = \sum_{i=1}^{k} w_i(j)T_i(j), \quad j = 1, 2, \ldots, N \tag{32}$$

where j is the index specifying individual pixels in the NOAA AVHRR images and N is the total number of pixels in the study area. The coverage ratios w_i's not only vary with landcover types but also pixels.

We also assume that within the study area the apparent temperatures of specific landcover types do not vary with spatial locations, i.e.,

$$T_i(j) = T_i, \quad j = 1, 2, \ldots, N. \tag{33}$$

where T_i's represent the landcover-specific apparent temperatures. Such assumption is reasonable since, for a specific landcover type, spatial variation of the apparent temperature within the study area (approximately 21 km × 13 km) is small, and more importantly the effect of landcover types on ambient air temperatures should be assessed on a region scale, not based on individual pixels. Thus, spatial variation of the pixel-average land surface temperatures depends on coverage ratios of different landcover types present in individual NOAA pixels, i.e.,

$$\bar{T}(j) = \sum_{i=1}^{k} w_i(j)T_i, \quad j = 1, 2, \ldots, N. \tag{34}$$

Or equivalently in matrix form,

$$\begin{bmatrix} \bar{T}(1) \\ \bar{T}(2) \\ \vdots \\ \bar{T}(N) \end{bmatrix} = \begin{bmatrix} w_1(1) & w_2(1) & \cdots & w_k(1) \\ w_1(2) & w_2(2) & \cdots & w_k(2) \\ & & \ddots & \\ w_1(N) & w_2(N) & \cdots & w_k(N) \end{bmatrix} \begin{bmatrix} T_1 \\ T_2 \\ \vdots \\ T_k \end{bmatrix} \tag{35}$$

$$\bar{T} = WT \tag{36}$$

In the above equation the pixel-average land surface temperatures ($\bar{T}$) can be substituted by the SWT surface temperatures, and thus if the coverage ratios $w_i (i = 1, 2, \ldots, k)$ are known, the landcover-specific surface temperatures $T_i (i = 1, 2, \ldots, k)$ can be determined by solving the inversion problem with the following least squares estimator:

$$T = (W'W)^{-1}W'\bar{T}. \tag{37}$$

The pixel-specific coverage ratios (W) were obtained by conducting a supervised landcover classification using high-resolution multispectral SPOT images and orthorectified aerial

photos. Implementation of the supervised landcover classification using remote sensing images involves the following steps:

(1) Determining the landcover types to be specified in the subsequent analysis. Both the landcover conditions present in the study area and the required level of landcover details should be taken into consideration. Four major landcover types—paddy fields (P), water ponds (W), built-up area and bare soils (B), and other vegetations (V) are present in the study area. However, there were also areas covered by clouds (C), and therefore, a total of five landcover types were specified.
(2) Determining the classification features to be used in classification. The selected features jointly should be able to differentiate different landcover types. SPOT multispectral (green, red, and near infrared) images were chosen as classification features in our study.
(3) Collecting training pixels of individual landcover types. This is done by making several field investigations and referencing to the aerial photos to identify areas on satellite images which are representative of different landcover types. Digital numbers of training pixels are then extracted to establish the spectral signatures of different landcover types. Such signatures characterize the distribution and variation of digital numbers of individual landcover types in the feature space and form the basis of supervised landcover classification.
(4) Pixels of unknown landcover types are classified by referencing their digital numbers to spectral signatures of different landcover types. Many classification methods have been developed and the maximum likelihood classification method was used in our study. Details of the supervised classification and the maximum likelihood classification method can be found in Schowengerdt (1997) and Schott (1997).

Results of landcover classification are assessed by the confusion matrix shown in Table 1. It achieves a very high overall accuracy (92.10%) and the user's and producer's accuracies of all landcover types except vegetations (V) are all higher than 86%. Table 1 shows some pixels belonging to paddy fields and vegetations are mutually misclassified since their spectral signatures are more similar. Particularly, vegetation pixels are more likely to be classified into paddy fields. Fig. 4 demonstrates the landcover image resulted from landcover classification using multispectral SPOT images.

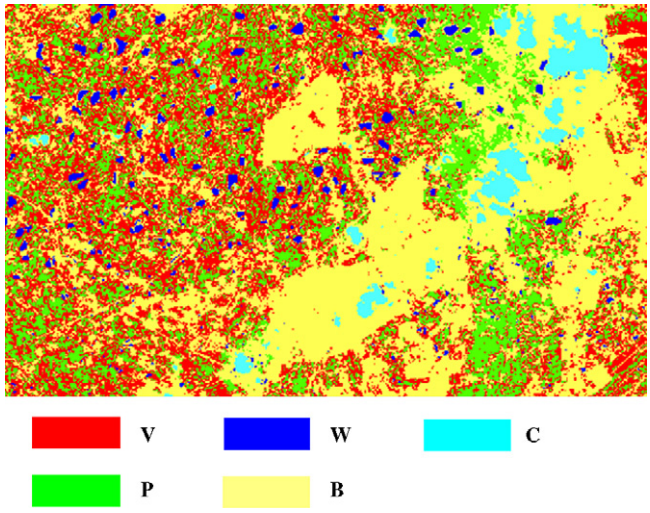

Fig. 4. Results of landcover classification using multispectral SPOT images. [W: water ponds, P: paddy fields, B: built-up, V: other vegetations, and C: clouds].

The landcover image derived from multispectral SPOT images has a spatial resolution of 20 m which is much smaller than the spatial resolution (1.1 km) of the NOAA AVHRR images. By overlaying NOAA AVHRR images on the landcover image (Fig. 4), the coverage ratios (W_i) of individual landcover types within each NOAA pixel can be determined and landcover-specific surface temperatures $T_i(i = 1,2,\ldots,k)$ can be obtained using Eq. (37). It should also be noted that NOAA pixels containing classified cloud pixels were excluded in subsequent analysis since coverage ratios of real landcover types in cloud-covered areas cannot be determined. As a result, among a total of 228 NOAA pixels, only 183 pixels ($N = 183$ in Eq. (35)) were used for estimation of landcover-specific surface temperatures.

Landcover-specific surface temperatures of the 2 days of field investigation (described in the Section 6) are shown in Table 2. Using the landcover-specific surface temperatures and within-pixel coverage ratios (W_i), pixel-average temperatures can be estimated by Eq. (35) and compared against the SWT surface temperatures. Fig. 5 demonstrates that pixel-average surface temperatures ($\bar{T}$) estimated by landcover-specific surface tem-

Table 1
Confusion matrix of the landcover classification using training data

	Reference landcover types					Sum	User's accuracy (%)
	W	P	B	V	C		
Classified landcover types							
W	3236	0	11	0	0	3247	99.66
P	0	3963	2	613	0	4578	86.57
B	98	1	5344	13	316	5772	92.58
V	4	487	26	1126	0	1643	68.53
C	0	0	88	0	5669	5757	98.47
Sum	3338	4451	5471	1752	5985	20997	Overall accuracy
Producer's accuracy (%)	96.94	89.04	97.68	64.27	94.72		92.10%

Table 2
Estimated landcover-specific surface and air temperatures (°C)

Date	Landcover type			
	W	P	B	V
Surface temperature				
03/16/2005	25.18	33.17	37.49	29.90
04/04/2005	20.84	28.88	33.31	24.65
Air temperature				
03/16/2005	26.35	28.51	29.34	27.77
04/04/2005	23.05	25.17	27.23	23.70

W: water ponds, P: paddy fields, B: built-up, V: other vegetations.

peratures and the SWT surface temperatures (T_{SWT}) are well correlated and the regression lines are almost identical to the line of equivalence (slope and interception of the regression lines are respectively very close to 1.0 and 0), suggesting the applicability of the landcover-specific surface temperatures and coverage ratios within individual NOAA pixels.

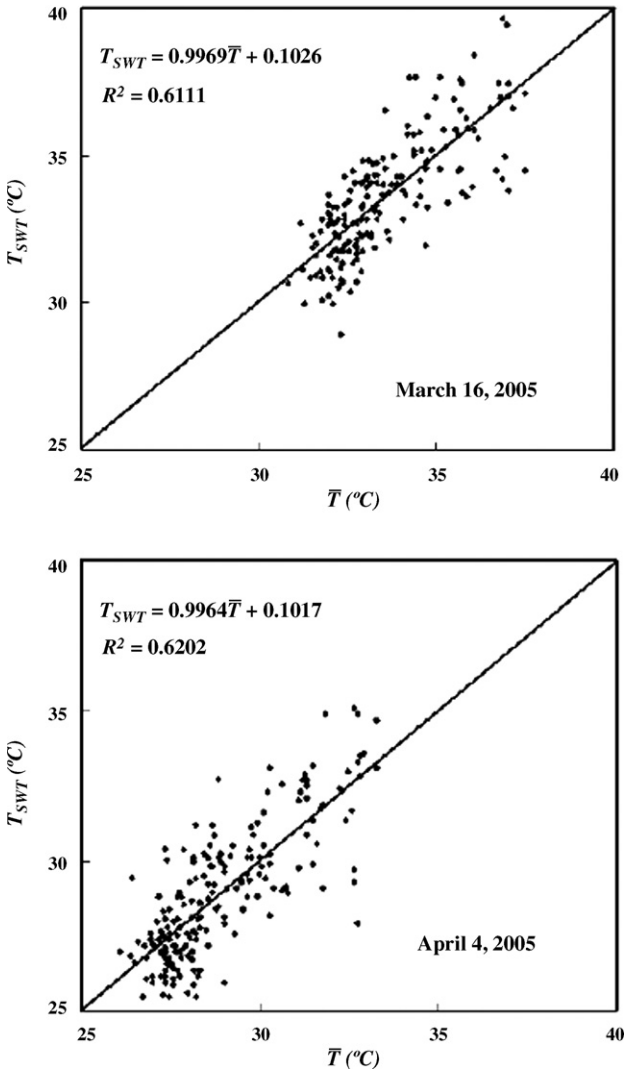

Fig. 5. Comparison of pixel-average surface temperatures derived by the split window technique (T_{SWT}) and estimated using landcover-specific surface temperatures ($\bar{T}$).

6. Pixel-average air temperature estimation

Field investigations were conducted on 16 March and 4 April 2005 in order to develop landcover-specific relationships for surface and air temperatures. During each trip of field investigation surface temperatures of different landcover types and corresponding air temperatures at 0.2, 0.4, 0.8, 1.2, 1.6 and 2 m above the ground surface were measured by an infrared thermometer. The field investigations were conducted roughly between 11:00 am and 2:30 pm in order to be nearly concurrent with the daytime overpass of NOAA AVHRR sensors. A V-shape sampling route as shown in Fig. 2 was adopted to take into consideration the spatial variation of temperatures and to cover both north–south and east–west extent of the study area. Land surface and air temperatures of different landcover types were measured at locations near centers of individual aerial photos (see Fig. 2) along the sampling route. At each location and height, 20 temperature readings were recorded and the average value was taken as the representative temperature. In order to take the diurnal temperature changes into consideration, a temperature adjustment practice suggested by Yokohari et al. (1997) was adopted. Upon completion of temperature sampling along the sampling route, land surface and air temperatures at the starting point were measured again and all other temperature measurements were adjusted to be consistent with the last measurement by assuming a linear temporal variation of temperatures. Fig. 6 illustrates vertical air temperature profiles of different landcover types.

Air temperatures above the surface of water ponds have reversed vertical profiles, i.e., the surface temperatures are lower than the air temperatures at different heights. For other landcover types, surface temperatures are higher than air temperatures. In particular, built-up areas have a sharp temperature decrease (about 6–12 °C) from the ground surface to 20 cm above the ground. Paddy fields and other vegetations have much smaller temperature decrease (about 0.5–3 °C) at the same height. More specifically, paddy fields seem to have a little larger temperature decrease than vegetations.

Using the above temperature measurements, the following empirical relationships (also shown in Fig. 7) of land surface temperature (T_s) and air temperatures at 2 m height (T_a) with respect to different landcover types were developed:

$$T_a = 0.7748T_s + 2.8106 \quad \text{(paddy field)} \tag{38a}$$

$$T_a = 0.505T_s + 10.407 \quad \text{(built} - \text{up)} \tag{38b}$$

$$T_a = 0.76T_s + 7.2131 \quad \text{(water ponds)} \tag{38c}$$

$$T_a = 0.7747T_s + 4.6043 \quad \text{(other vegetations)} \tag{38d}$$

These relationships are needed for calculation of NOAA-pixel-average air temperatures using a procedure illustrated in Fig. 8 and described below.

Spatial variation of surface temperatures within a NOAA pixel is characterized by the landcover-specific surface temperatures and spatial distribution of different landcover types within the NOAA pixel. The landcover-specific surface temperatures are then converted to landcover-specific air temperatures

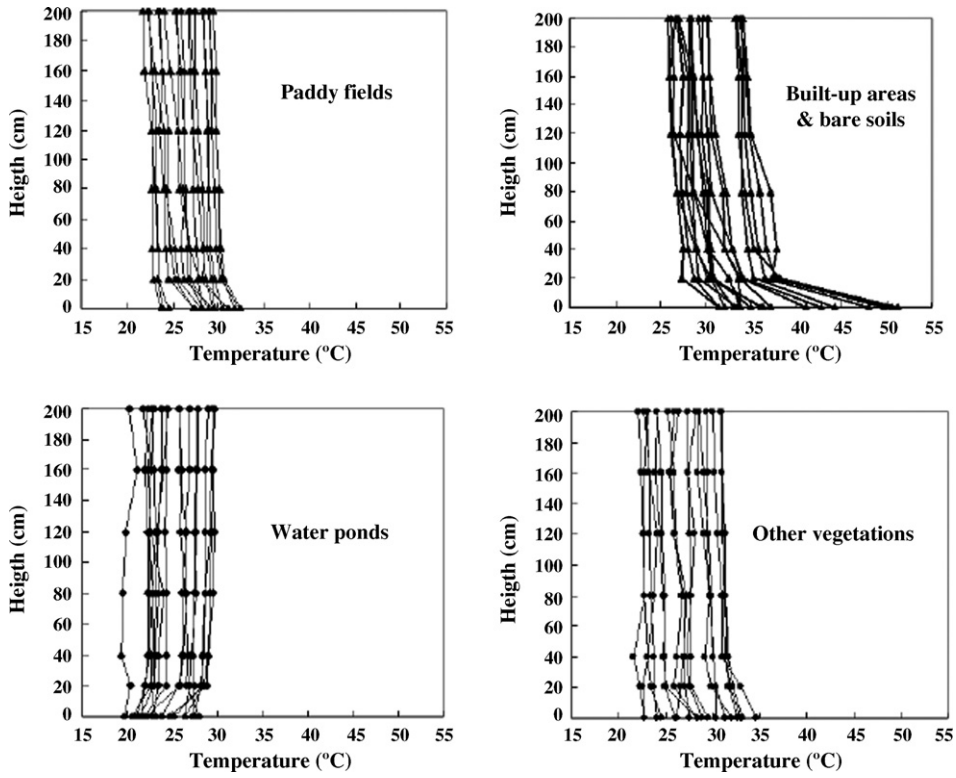

Fig. 6. Vertical temperature profiles of different landcover types.

using the empirical relationships of Eqs. (38a)–(38d). Although empirical relationships between the surface temperatures and air temperatures were derived based on point temperature measurements, they were also used for converting the landcover-specific surface temperatures (which represent area-average temperatures) to corresponding air temperatures. Finally, the average air temperatures over individual NOAA pixels were calculated as the area-weighted average of landcover-specific air tempera-

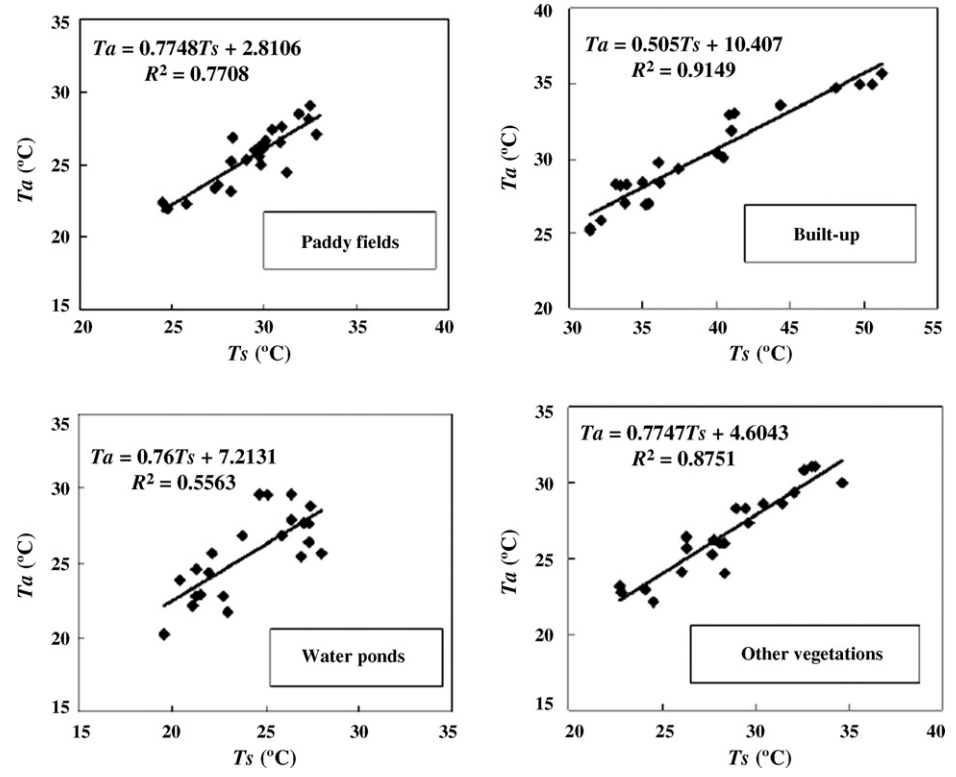

Fig. 7. Landcover-specific empirical relationships between the air temperature at 2 m height (T_a) and surface temperature (T_s).

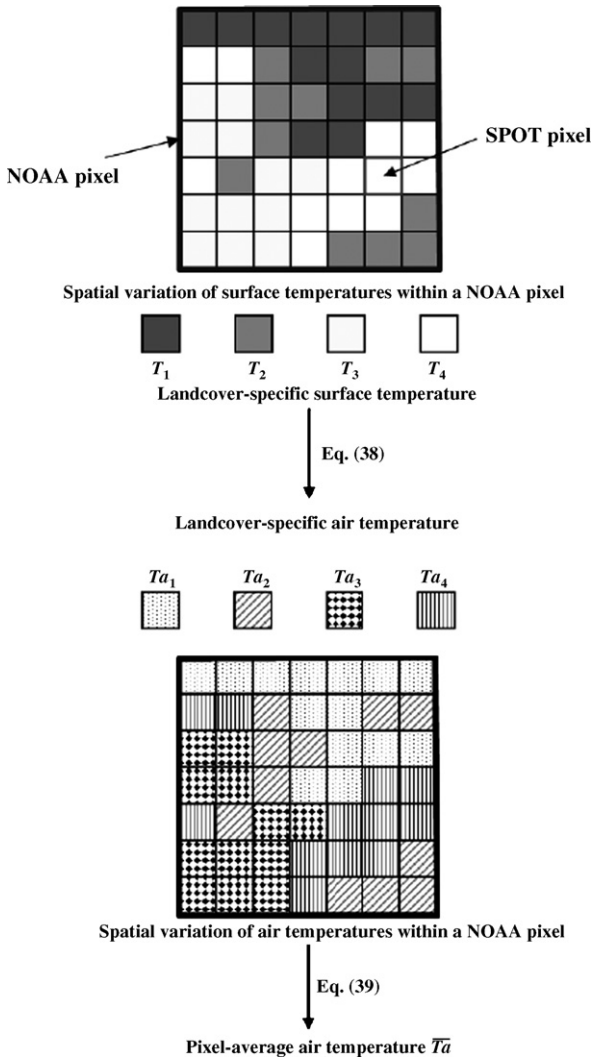

Fig. 8. Schematic illustration of procedures for calculation of pixel-average air temperature over a NOAA pixel.

tures, i.e.,

$$\overline{T_a}(j) = \sum_{i=1}^{k} w_i(j) T_{a_i}, \quad j = 1, 2, \ldots, N. \tag{39}$$

where $\overline{T_a}(j)$ is the average air temperature of the jth NOAA pixel, T_{a_i} the air temperature of the ith landcover type, and $w_i(j)$ represents the coverage ratio of the ith landcover type presents in the jth NOAA pixel.

Table 2 shows the landcover-specific air temperatures at the time of field investigation estimated using the above method. Readers are reminded that the average surface and air temperatures discussed in this paper refer to respective average temperatures over individual NOAA pixels. We consider the size of a NOAA pixel (1.1 km × 1.1 km) is appropriate for assessing the landcover changes and its effect on ambient air temperatures.

7. Effect of landcover types on ambient air temperatures

Table 2 indicates that surface temperatures vary with landcover types. Built-up areas with paved roads and residential and factory buildings have significant higher surface temperatures than other landcover types, while water ponds have the lowest surface temperatures. Surface temperatures of paddy fields are 3–4° higher than that of other vegetations. This may be due to the fact that rice crops in the paddy fields have not formed full canopy coverage at the time of this study. However, with regard to the living environment, it is the ambient air temperature that is of major concern.

Although the built-up landcover has a significantly higher surface temperature than other landcover types, the corresponding air temperature differences are smaller. This is because the built-up landcover has the largest vertical temperature gradient. On 16 March 2005 the maximum air temperature difference (between the built-up areas and the water ponds) was about 3 °C, while on 4 April 2005 the maximum difference was about 4.2 °C. It is worthy to mention that the differences between landcover-specific surface and air temperatures are also dependent on local climatological condition.

The data in Table 2 imply that if an area of NOAA pixel size (1.1 km × 1.1 km) with a complete water ponds coverage is converted to a complete built-up coverage, the ambient air temperature will be raised by about 3 °C (29.34 − 26.35) to 4 °C (27.23 − 23.05). Other kinds of landcover conversions will result in smaller changes on ambient air temperatures. Similarly, if the same area is converted from a full paddy coverage to a complete built-up area, the ambient air temperature rise will be about 0.8 °C (29.34 − 28.51) to 2 °C (27.23 − 25.17). Such arbitrarily hypothesized landcover conversions between two landcover types are referred to as the blind landcover conversions since it may not reflect the actual landcover conditions of the study area. For example, in our study there is no pixel with complete paddy or water coverage.

We argue that landcover conversions will not arbitrarily occur and the likely conversions are often restricted by the local or regional conditions of resources availability, transportation, etc. Within an area of NOAA pixel size, landcover conversions are more likely to take place among several landcover types, instead of mutual conversion between two landcover types. Prevalent landcover conversions are related to climatological, geographical, economical, sociological, and other factors, and should be considered in assessing the effect of landcover types on ambient air temperatures. Such prevalent conversions often are too complicated to be characterized by a generally applicable model and should be considered as a local or regional phenomenon. Thus, a locally based assessment of the effect of landcover types on ambient air temperatures is presented below.

Apart from comparing the landcover-specific air temperatures based on blind landcover conversions, another way of assessing the effect of landcover types on ambient air temperatures is by evaluating average air temperatures with respect to coverage ratios of certain landcover types within individual NOAA pixels. Such assessment is similar to Yokohari et al.

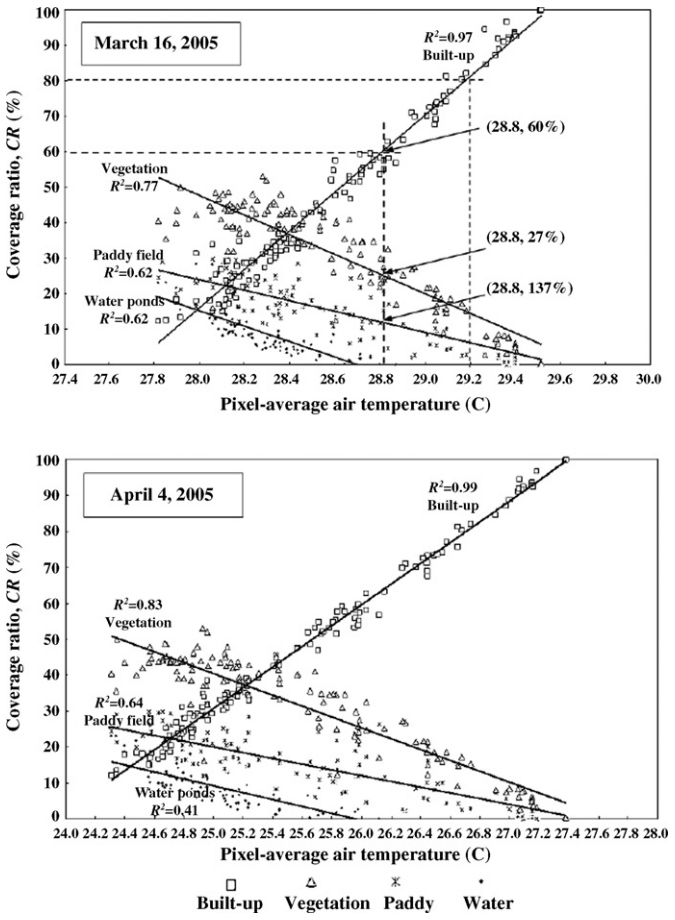

Fig. 9. Empirical relationships between within-pixel coverage ratios of different landcover types and pixel-average air temperatures. The inter-related regression lines collectively characterize the prevalent landcover conversion pattern of the study area.

(1997), although in their study temperature differences between 50 m × 50 m cells and a reference urban area with respect to paddy coverage ratios were evaluated.

Fig. 9 illustrates relationships between pixel-average air temperatures ($\overline{T}_a$) and within-pixel coverage ratios (CR) of different landcover types. All regression lines, particularly the one associated with the built-up landcover type, are very significant, suggesting well-established landcover patterns in the study area. It should be emphasized that, for any given value of average air temperature (e.g., 28.8 °C), the sum of corresponding coverage ratios of different landcover types (determined by the regression lines) is always very close to 100%. It indicates the regression lines shown in Fig. 9 are inter-related and collectively they characterize the existing landcover pattern within the study area. For example, a pixel with 60% built-up coverage is likely to have about 27 and 13% coverages of vegetations and paddy fields, respectively. The maximum coverage ratio of paddy fields within a NOAA pixel is about 26% whereas the maximum coverage ratio of built-up areas reaches near 100% due to the dense population and fully developed industrial and manufactural parks. It can also be observed that water ponds only exist in areas which are agriculture (paddy fields and other vegetations combined) dominant since they are used as irrigation water supply. Another important observation of Fig. 9 is that reduction in paddy and vegetation coverages tend to occur contemporaneously due to decline in agricultural activities, and such reductions are converted to increase of built-up areas. For regions with no well-established landcover pattern, co-existence of the landcover-specific regression lines in Fig. 9 will not appear.

The increasing (or decreasing) trend of ambient air temperatures with respect to increasing within-pixel coverage ratio of built-up areas (or other landcover types) is apparent. Under the existing landcover pattern (i.e., the pattern of inter-related regression lines in Fig. 9), the ambient air temperature will rise by 1.7 °C (from 27.8 to 29.5 on 16 March) to 3.1 °C (from 24.3 to 27.4 on 4 April) if the coverage ratio of paddy fields decreases from its maximum of 26% to none. It may seem unreasonable that this amount of ambient air temperature rise is higher than the 0.8–2 °C rise under the blind landcover conversion. This can be explained by considering the existing landcover pattern in the region.

Under the existing landcover pattern of the study area, a pixel with 26% paddy coverage is likely to have 19% water ponds, 51% vegetations, and only 5% of built-up area, resulting in a pixel-average air temperature of 27.8 °C (16 March 2005) which is lower than the landcover-specific air temperature of paddy fields (28.51 °C). Similarly, when the paddy coverage is reduced to zero, the vegetation coverage will also decrease due to decline of agricultural activities in the area. Reduced coverages of paddy fields and vegetations are converted to built-up areas, causing the pixel-average air temperature to reach around 29.5 °C (very close to the landcover-specific air temperature for built-up areas, 29.34 °C). The well-established existing landcover pattern reflects the complex local conditions that sustain the totality of the living environment in the region. Blind landcover conversion ignores such existing landcover pattern and will only yield imaginary assessment results. For example, assessing the effect of turning huge areas (several pixels) of all-paddy fields into water ponds is unrealistic since such all-paddy pixels do not exist in the study area. Scenarios contradicting the existing landcover pattern should not be presented for assessment.

We may further consider the situation of changing from an existing landcover condition to a forced landcover condition. Suppose a pixel with existing landcover condition of 26% paddy fields is forced to become 50% of built-up areas and 50% of paddy fields. Under such forced landcover conversion, the average air temperature will be raised from 27.8 to 28.93 °C (using landcover-specific air temperatures on 16 March 2005), an increase of 1.13 °C. In contrast, if a prevalent landcover conversion (conversion following the existing landcover pattern) is taken, a pixel with 50% built-up coverage (corresponding to 16% and 32% coverages of paddy fields and other vegetation, respectively) has an average air temperature of 28.63 °C. The forced conversion results in a higher temperature increase than would be under prevalent conversion.

The concept of different landcover conversions can be better illustrated in a coverage-ratio space as shown in Fig. 10. Scattering of actual landcover ratios of individual NOAA pixels (points marked by ▲ except C and D) exhibits a pattern which characterizes the existing landcover conditions. Landcover condition of

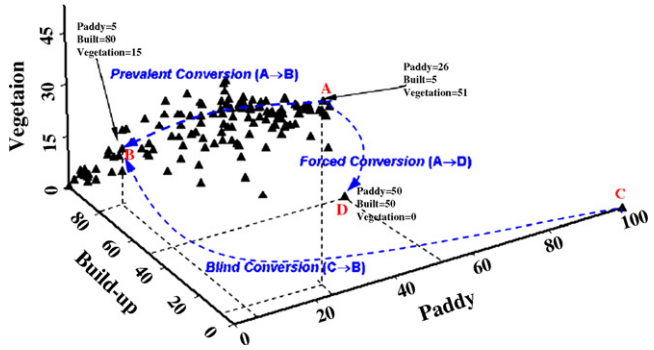

Fig. 10. Illustrative example of the prevalent, blind and forced conversions. Numbers represent coverage ratios in percentage. Points marked by ▲ (except C and D) represent actual landcover coverage ratios of NOAA pixels in the study area. Scattering of these points characterizes the existing landcover pattern.

point C is unrealistic and thus landcover conversion from point C to B is a blind conversion. Point A represents an existing landcover condition and conversions from point A to B and D are respectively the prevalent and forced landcover conversions. A forced landcover conversion contradicts the existing landcover pattern and may cause complicated consequences. For instance, conversion from point A to D will force landcover types of vegetation and water ponds to disappear and increase the coverage of paddy fields and built-up areas. It may encounter problems such as not having enough water for irrigation and low intention of local farmers to transform from vegetation growing to paddy culture. Additional resources allocation and incentives may need to be introduced in order to ensure a successful forced conversion.

Several final remarks should also be mentioned:

(1) We recognize that environmental changes are dynamic processes and the existing landcover pattern may gradually change over time. Therefore, long-term monitoring of landcover changes should be pursued.
(2) Analyses and results of this pilot study were based on data collected in only 2 days of field investigation. It may not reflect the complete range of temperature changes during the full growing period of paddy rice. Therefore, continuation of this pilot study is necessary for a more complete assessment of landcover effect on ambient air temperature in the study area.
(3) Spatial scattering of different landcover types within a NOAA pixel may also affect the pixel-average air temperatures. Yokohari et al. (1997) studied the effect of segmentation of paddy fields on air temperature and found that, for intermediate coverage ratios (30–70%) of paddy fields, segmentation level of paddy fields has strong influence on air temperature. However, spatial scattering (or segmentation) involves four different landcover types and their overall effect on air temperatures is more complicated and should be pursued in future study.

8. Conclusions

In this study we present a new method for assessment of landcover effect on ambient air temperature using remote sensing images. The proposed method takes into account the existing landcover pattern. A few concluding remarks are drawn as follows.

Landcover-specific empirical relationships exist between within-pixel coverage ratios and pixel-average air temperatures. These empirical relationships are inter-related and they collectively characterize the existing landcover pattern of the region.

Landcover conversions tend to follow a local prevalent pattern which sustains the totality of the living environment in the region.

In our study, under the prevalent landcover conversion pattern, reducing the coverage ratio of paddy fields from its maximum of 26% to none will result in an ambient air temperature rise of 1.7–3.1 °C.

Increasing the coverage ratio of built-up areas (or decreasing coverages of paddy fields, other vegetations, and water ponds) will result in rise of ambient air temperatures (measured at 2 m height).

In the study area, reductions in paddy and vegetation coverage tend to occur contemporaneously due to the decline in agricultural activities, and such reductions are converted to increase of built-up areas.

Acknowledgements

We are thankful to the Central Weather Bureau of Taiwan, ROC for providing NOAA AVHRR images for this study. The first author is also grateful for the National Science Council of Taiwan, ROC and the Kyoto University, Japan for providing financial and facilitary supports for his sabbatical leave at the Kyoto University during which this manuscript was prepared.

References

Chedin, H., Scott, N.A., Berroir, A., 1982. A single channel double-viewing angle method for sea surface temperature determination from coincident METEOSAT and TIROS-N radiometric measurements. J. Climate Appl. Meteorol. 21, 613–618.

Florio, E.N., Lele, S.R., Chang, Y.C., Sterner, R., Glass, G.E., 2004. Integrating AVHRR satellite data and NOAA ground observations to predict surface air temperature: a statistical approach. Int. J. Remote Sens. 25, 2979–2994.

Fukuda, S., Hiramatsu, K., Mori, M., 2006. Fuzzy neural network model for habitat prediction and HEP for habitat quality estimation focusing on Japanese medaka (*Oryzias latipes*) in agricultural canals. Paddy Water Environ. 4, 119–124.

Gallo, K.P., McNab, A.L., Karl, T.R., Brown, J.F., Hood, J.J., Tarpley, J.D., 1993. The use NOAA AVHRR data for assessment of the urban heat island effect. J. Appl. Meteorol. 32, 899–908.

Greppi, M., 2004. Infiltration process and groundwater table rising in a paddy field area. Paddy Water Environ. 2, 171–179.

Idso, S.B., Jackson, R.D., Reginator, R.J., 1997. Remote sensing of crop yields. Science 196, 19–25.

Ishikawa, M., Tabuchi, T., Yamaji, E., 2003. Clarification of adsorption and movement by predicting ammonia nitrogen concentrations in paddy percolation water. Paddy Water Environ. 1, 27–33.

Kerr, Y.H., Lagouarde, J.P., Imbernon, J., 1992. Accurate land surface temperature retrieval from AVHRR data with use of an improved split window algorithm. Remote Sens. Environ. 41, 197–209.

Li, Z.L., Becker, F., 1993. Feasibility of land surface temperature and emissivity determination from AVHRR data. Remote Sens. Environ. 43, 67–85.

McMillan, L.M., 1975. Estimation of sea surface temperatures from two infrared window measurements with different absorptions. J. Geophys. Res. 80, 5113–5117.

Monteith, J.L., Unsworth, M.H., 1990. Principles of environmental physics. Edward Arnold.

Nakanishi, N., 2004. Potential rainwater storage capacity of irrigation ponds. Paddy Water Environ. 2, 91–97.

Nakasone, H., 2003. Runoff water quality characteristics in a small agriculture watershed. Paddy Water Environ. 1, 183–188.

Prabhakara, C., Dalu, G., Kunde, V.G., 1974. Estimation of the sea surface temperature from remote sensing in the 11 to 13 μm window region. J. Geophys. Res. 79, 5039–5044.

Price, J.C., 1984. Land surface temperature measurements from the split window channels of the NOAA 7 advanced very high-resolution radiometer. J. Geophys. Res. 89, 7231–7237.

Saptomo, S.K., Nakano, Y., Yuge, K., Haraguchi, T., 2004. Observation and simulation of thermal environment in a paddy field. Paddy Water Environ. 2, 73–82.

Schott, J.R., 1997. Remote Sensing—the Image Chain Approach. Oxford University Press.

Schowengerdt, R.A., 1997. Remote Sensing—Models and Methods for Image Processing. Academic Press.

Unami, K., Kawachi, T., 2005. Systematic assessment of flood mitigation in a tank irrigated paddy fields area. Paddy Water Environ. 3, 191–199.

Vasquez, D.P., Reyes, F.J.O., Arboledas, L.A., 1997. A comparative study of algorithms for estimating land surface temperature from AVHRR data. Remote Sens. Environ. 62, 215–222.

Yokohari, M., Brown, R.D., Takeuchi, K., 1994. A framework for the conservation of rural ecological landscapes in the urban fringe area in Japan. Landscape Urban Plan. 29, 103–116.

Yokohari, M., Brown, R.D., Kato, Y., Moriyama, H., 1997. Effect of paddy fields on summertime air and surface temperatures in urban fringe areas of Tokyo, Japan. Landscape Urban Plan. 38, 1–11.

Yokohari, M., Brown, R.D., Kato, Y., Yamamoto, S., 2001. The cooling effect of paddy fields on summertime air temperature in residential Tokyo, Japan. Landscape Urban Plan. 53, 17–27.